Photoreceptors Degenerate Through Pyroptosis After Experimental Retinal Detachment

Xiaomeng Li,[1] Yang Liu,[1] Mengsha Sun,[1] Min Gao,[1] Tong Li,[1] Jian Liang,[1,2] Yuanqi Zhai,[1,3] Mengqiao Xu,[1] Xiangjun She,[1] Shiqi Yang,[1] Wenjia Liu,[1] Xueting Luo,[1,2] and Xiaodong Sun[1–3]

[1]Department of Ophthalmology, Shanghai General Hospital (Shanghai First People's Hospital), Shanghai Jiao Tong University School of Medicine, Shanghai, People's Republic of China
[2]Shanghai Key Laboratory of Fundus Diseases, Shanghai, People's Republic of China
[3]Shanghai Engineering Center for Visual Science and Photomedicine, Shanghai, People's Republic of China

Correspondence: Xiaodong Sun, Department of Ophthalmology, Shanghai First People's Hospital, Shanghai Jiao Tong University School of Medicine, 100 Hai Ning Road, Shanghai 200080, People's Republic of China; xdsun@sjtu.edu.cn.
Xueting Luo, Department of Ophthalmology, Shanghai First People's Hospital, Shanghai Jiao Tong University School of Medicine, 100 Hai Ning Road, Shanghai 200080, People's Republic of China; xtluo@sjtu.edu.cn.

XiL and YL contributed equally to the work presented here and should therefore be regarded as equivalent authors.

Received: January 9, 2020
Accepted: June 16, 2020
Published: July 22, 2020

Citation: Li X, Liu Y, Sun M, et al. Photoreceptors degenerate through pyroptosis after experimental retinal detachment. *Invest Ophthalmol Vis Sci.* 2020;61(8):31. https://doi.org/10.1167/iovs.61.8.31

Purpose. Gasdermin D (GSDMD) is crucial in neuronal pyroptosis. GSDMD-N and GSDMD-C are two subdomains of the protein GSDMD. GSDMD-N is an executor of pyroptosis, and GSDMD-C has an inhibitory effect on pyroptotic cell death. This study evaluated the role of GSDMD in photoreceptor cell pyroptosis caused by retinal detachment (RD).

Methods. RD models were established in rats, and GSDMD cleavage was detected by western blotting. The morphology of photoreceptors was assessed by transmission electron microscopy. Some rats were given subretinal injections of recombinant adeno-associated virus 2/8 (rAAV2/8)–GSDMD-C before RD surgery. We documented the expression of caspase-1 and GSDMD-N in retinas by western blot. Levels of IL-1β, TNF-α, and monocyte chemoattractant protein-1 (MCP-1) were detected by quantitative RT-PCR. The membrane integrity of photoreceptors was evaluated by TOTO-3 iodide staining. Retinal function was measured by electroretinography, and the thickness of the outer nuclear layer was also recorded. We measured the activation of glial fibrillary acidic protein (GFAP), F4/80, and ionized calcium binding adaptor molecule 1 (Iba-1) by immunofluorescence.

Results. The cleavage of GSDMD peaked at 1 day after RD. The administration of rAAV2/8–GSDMD-C reduced the pyroptosis and subsequent apoptosis of photoreceptors and preserved the retinal function after RD. Expression of IL-1, TNF-α, and MCP-1 was decreased in the rAAV2/8–GSDMD-C group. In addition, the activation of GFAP, Iba-1, and F4/80 in retinas was alleviated by administering rAAV2/8–GSDMD-C after RD.

Conclusions. GSDMD participates in the pyroptosis of photoreceptor after RD. Overexpression of GSDMD-C may block GSDMD cleavage and attenuate photoreceptor degeneration.

Keywords: retinal detachment, photoreceptors, pyroptosis, Gasdermin D

Retinal detachment (RD), characterized by separation of the neurosensory retina from the retinal pigment epithelium (RPE), is a relatively common cause of visual impairment.[1] Although intraocular reparative surgery has been developed to achieve anatomical reattachment, 60% of patients with rhegmatogenous retinal detachment involving the macula (50% of the cases) have less than 20/40 vision after surgery, and a poor vision-related quality of life persists.[2] Retinal degeneration has been recognized as a key factor responsible for vision decline. Currently, no neuroprotective strategy is available to halt retinal degeneration under disease conditions. Thus, elucidation of the molecular mechanisms underlying retinal degeneration after RD is a prerequisite for the rational design of therapeutic interventions.

Neuroretina is metabolically nourished by the RPE and choroidal microvasculature.[3] Maintenance of intimate structures between the neuroretina and RPE is critical to retinal physiology and homeostasis,[3,4] and disruption of the retina–RPE complex would disturb retinal homeostasis in severe cases of photoreceptor degeneration.[5] Previous studies have shown that inhibition of the apoptotic pathway does not efficiently halt photoreceptor degeneration, due to activation of other death pathways, such as necroptosis.[6,7] Although interventions aimed at both apoptotic and necrotic pathways were shown to substantially preserve photoreceptors after experimental RD,[8] photoreceptor death still persisted.[7,9] Therefore, more complicated degenerative cascades might be involved in RD-induced retinal degeneration.

Pyroptosis is a programmed cell death pathway characterized by plasma membrane permeabilization, cell swelling, and lysis.[10] Pyroptosis is regulated by inflammatory caspases, including caspase-1, −4, −5, and −11.[11,12] Mechanistically, active caspases cleave gasdermin D (GSDMD), a latent cytoplasmic molecule, and release the inhibitory

C-terminal moiety, which results in activation of the N-terminal domain with intrinsic membrane-insertional and pore-forming activity.[13–15] Insertion of GSDMD-N moieties into the plasma membrane and subsequent assembly of non-selective pores resulted in membrane disruption and cell lysis.[16] Thus, cleavage of GSDMD is regarded as a marker for pyroptosis activation.

Previous studies have found that inflammatory molecules, such as IL-1β and caspase-1, are upregulated in subretinal fluids and vitreous samples of RD patients.[17] Similar findings were also reported in disease models.[17] However, whether pyroptosis is involved in RD-induced retinal degeneration has not been explored. We aimed to study whether pyroptosis is an alternative degenerative pathway involved in photoreceptor death after experimental RD in rats.

Materials and Methods

rAAV2/8–GSDMD-C Virus

The C-terminal part of GSDMD was cloned from rat placenta cDNA with the primers 5′-AGATCGTGGATCATGCCGTC-3′ and 5′-TGAGTCACACGCAGCATACA-3′. A hemagglutinin (HA) tag was added in frame to the C-terminus of GSDMD by PCR. The HA-tagged GSDMD-C construct was subcloned into the pAAV-MCS vector (Stratagene, Cedar Creek, TX, USA) downstream of the cytomegalovirus promoter/β-globin intron enhancer. The final recombinant adeno-associated virus 2/8 (rAAV2/8)–GSDMD-C construct was verified by Sanger sequencing. To package the rAAVs, pAAV-RC and pHelper plasmids (Stratagene) were also used for cotransfection of 293T cells. The AAV viral particles were purified by a fast protein liquid chromatography method, which resulted in viral titers of approximately 4×10^{12} vg/mL. A construct expressing green fluorescent protein (GFP), rAAV2/8–eGFP, was used as a control.

Animals and Virus Injection

All animal experiments were approved by the Animal Research Committee at Shanghai Jiaotong University and conducted with strict adherence to the ARVO Statement for the Use of Animals in Ophthalmic and Vision Research. Brown-Norway rats (male; ages 7–8 weeks; weight 260–280 g) were provided by the Shanghai First People's Hospital of Shanghai Jiao Tong University. The rats were raised in standard cages, with three or four animals per cage. Rats were kept in standard housing conditions with free access to food and water; the temperature was maintained at 25°C under a 12-hour light/dark cycle. For experimental use, rats were randomly divided into five groups: control, RD, RD + balanced salt solution (BSS), RD + rAAV2/8–GSDMD-C, and RD + rAAV2/8–eGFP. At least six rats in each repetition were used for analysis. All animal experiments were repeated three times.

All surgical procedures were performed only on the right eyes of the rats, and the contralateral left eyes were reserved as control eyes. Subretinal injection was performed as previously described.[7] Briefly, rats were anesthetized by intraperitoneal injection with 1% sodium pentobarbital (Sigma-Aldrich, St. Louis, MO, USA) at a dose of 30 mg/kg body weight. Before surgery, the pupils were dilated with 0.5% tropicamide and 0.5% epinephrine (Santen Pharmaceutical Co., Ltd., Osaka, Japan). Through microscopy, a corneal contact lens was placed directly on the rat cornea, and the sclera and choroid were punctured with a 30-gauge needle. An injection of rAAV2/8–GSDMD-C (5 µL, 4×10^{12} vg/mL) was slowly introduced into the subretinal space with a 32-gauge needle, and a slight bulge was observed in the rat fundus. Control rats received 5 µL subretinal injection of rAAV2/8–eGFP and BSS in the same way. Levofloxacin eyedrops were applied three times a day for three days after subretinal injection to prevent potential ocular infections.

RD Surgery

RD surgery was performed three weeks after virus injection as previously described.[18] Briefly, the rats were anaesthetized via intraperitoneal injections of sodium pentobarbital at a dose of 30 mg/kg body weight. Pupils were dilated with 0.5% tropicamide and 0.5% epinephrine (Santen Pharmaceutical). Under an anatomic microscope, we used a 27-gauge needle to create a self-sealing scleral incision 1.5 mm posterior to the corneal limbus. The needle's bevel was pointed up to avoid damaging the lens. Through sclerotomy, a small area of the peripheral retina was carefully lifted with a 30-gauge needle. Sodium hyaluronate (10 mg/mL; LG Life Sciences, Seoul, Korea) was slowly injected into the subretinal space until approximately two-thirds of the neurosensory retina was detached from the underlying RPE. The scleral wounds of the rats were then smeared with ofloxacin antibiotic ointment (Dikeluo; Siqi Pharmaceutical Co., Ltd., Shenyang, China). The rats rested on a heating pad to prevent hypothermia. Levofloxacin eyedrops were applied three times a day for 3 days after RD surgery to prevent potential ocular infections.

Immunofluorescence

Rats were sacrificed and transcardially perfused with 4% paraformaldehyde. The eyeballs were harvested and dehydrated with 30% sucrose solution for 5 hours and were fully embedded in Tissue OCT-Freeze Medium (Sakura Finetek, Tokyo, Japan) at –20°C. Retinal sections were cut at a thickness of 10 µm and blocked in 10% goat serum for 1 hour. The sections were then incubated with the following primary antibodies at 4°C overnight: caspase-1 (1:200; cat. no. AB1871, Sigma-Aldrich), HA (1:300; cat. no. 3724S, Cell Signaling Technology, Danvers, MA, USA), ionized calcium binding adaptor molecule 1 (Iba-1) (1:300; cat. no. ab5076; Abcam, Cambridge, UK), F4/80 (1:300; cat. no. ab6640, Abcam), and glial fibrillary acidic protein (GFAP, 1:150; cat. no. ab7260, Abcam). After the sections were thoroughly washed with PBS, they were incubated with Alexa Fluor 594 Goat Anti-Rabbit IgG H&L antibody (1:1000; cat. no. ab150088, Abcam) for 1 hour at room temperature. Finally, the sections were counterstained with 4′,6-diamidino-2-phenylindole (DAPI), washed again, coverslipped, and examined under a confocal microscopy (TCS SP8; Leica, Wetzlar, Germany).

Membrane Integrity Evaluation

The membrane integrity of photoreceptor cells was evaluated by TOTO-3 iodide (cat. no. T3604; Life Technologies, Carlsbad, CA, USA) staining. Subretinal injections of TOTO-3 were performed 1 day after RD induction. In brief, TOTO-3 iodide was dissolved in BSS to a final concentration of 50 µg/mL and then injected into the subretinal

Investigative Ophthalmology & Visual Science

space (5 µL) 2 hours before sacrifice. After enucleation of the eyeballs, cryosections were cut at 10 µm. The TOTO-3-labeled sections were fixed with 100% ethanol for 10 minutes at room temperature. The cell nuclei were then stained with DAPI. The retinal sections were photographed by confocal microscopy (Leica TCS SP8). At least three representative sections were selected per eye. The number of TOTO-3-positive cells was assessed from three non-overlapping regions, which were randomly selected at the maximal height of RD by blinded observers.

Electroretinography

Retinal function was examined by electroretinography with overnight dark adaptation before and 7 days after RD. All of the procedures were performed in dim red light. Briefly, the pupils of the rats were dilated after anesthetization as previously described. A gold wire electrode was placed on the cornea, a reference electrode was placed on the head, and the tail was connected with a ground electrode. The photic stimulation induced by a light flash (3.0 cd·s/m^2) was amplified; the preamplifier bandwidth was set at 0.2 to 300 Hz. The a-wave was measured from the baseline to the maximum initial negative response, and the b-wave was measured from the peak of the a-wave to the positive peak. Baseline electroretinograms (ERGs) were recorded 3 weeks after virus injection.

Western Blot Analysis

The retinas were homogenized with lysis buffer containing 50-mmol/L Tris 7.4, 150-mmol/L NaCl, 1% Triton X-100 (Sigma-Aldrich), 1% sodium deoxycholate, 0.1% SDS, and inhibitors of protease (cat. no. 11679498001; Roche, Mannheim, Germany) and phosphatase (cat. no. P0044, Sigma-Aldrich). The samples were run on 8% to 12% Bis-Tris gel electrophoresis and then electrotransferred onto polyvinylidene fluoride membranes. The membranes were blocked by incubation with 5% BSA in Tris-buffered saline and 0.02% Tween-20 (pH 7.4; Sigma-Aldrich) for 2 hours at room temperature. The blotting membranes were reacted with GSDMD antibody (1:1000; cat. no. G7422, Sigma-Aldrich), which specifically binds to the N-terminal of the molecule[14]; caspase-1 (1:1000; cat. no. 89332, Cell Signaling Technology), HA (1:1000; cat. no. 3724S, Cell Signaling Technology); IL-1β (1:1000; cat. no. ab9722, Abcam); and glyceraldehyde 3-phosphate dehydrogenase (GAPDH, 1:1000; cat. no. AF1186, Beyotime Institute of Biotechnology, Jiangsu, China) antibodies at 4°C overnight. They were then rinsed three times and incubated with the corresponding horseradish peroxidase-labeled secondary antibodies for 1 hour at room temperature. Protein bands were visualized using enhanced chemiluminescence (Amersham Pharmacia Biotech, Amersham, UK). Signal density was quantified using ImageJ 1.48 software (National Institutes of Health, Bethesda, MD, USA).

Transmission Electron Photomicrographs in the Outer Nuclear Layer

We used transmission electron microscopy (TEM) to observe RD-induced morphologic alterations in the photoreceptors. Briefly, the rats were sacrificed 1 day and 3 days after RD, and the eyes were enucleated. The corneas were then rapidly removed along the limbus. The detached retinas were carefully separated and immediately immersed in cold (4°C) 4% glutaraldehyde (0.1-mol/L phosphate buffer, pH 7.4) solution and incubated for 24 hours. The retinas were then dissected and fixed with 1% osmium tetroxide in 0.1-mol/L sodium phosphate buffer (pH 7.2), after which the samples were dehydrated in ethanol and water and embedded in eponate. TEM sections were stained with lead citrate for 10 minutes, washed with double-distilled water (ddH_2O) three times, stained with uranium acetate for 30 minutes, washed again with ddH_2O three times, and then observed by transmission electron microscope. The samples were assessed and photographed using a JEM-1200EX electron microscope (JEM, Tokyo, Japan). Twelve non-overlapping regions in all four quadrants of each retina sample were photographed and subjected to quantification of cell death modes. Typically, photoreceptors associated with cellular and organelle swelling and discontinuities in the plasma and nuclear membrane were defined as pyroptotic and necrotic cells, whereas photoreceptors showing cellular shrinkage and nuclear condensation were defined as apoptotic cells.

Histopathological Retinal Outer Nuclear Layer Thickness Assessment

Paraffin retinal sections (10 µm) were cut and stained with hematoxylin and eosin (H&E). The area of most detached retina was photographed (the retina was photographed under a Confocal microscope magnified 20 times) for measurement. The outer nuclear layer (ONL) thickness, from the outer segments (OSs) to the interior of the ganglion cell layer nuclei, and retinal thickness were analyzed every 300 µm by blinded observers. Separation of the RPE and the OSs was recognized as a detached retina. Retinal thickness was standardized (detached retina thickness ÷ attached retina thickness). As for the ratio of ONL measurements, thickness was standardized using the formula (ONL detached ÷ total retina detached)/(ONL attached ÷ total retina attached). Observers were masked during the whole measurements and calculations.

Reverse Transcription PCR

Total RNA was extracted from whole retinas by a Total RNA Extraction Kit (Tiangen, Beijing, China). The extracted RNA from each group was reverse transcribed into cDNA using a Synthesis Kit (Takara, Shiga, Japan). Quantitative RT-PCR (qRT-PCR) was performed using a qPCR Detection Kit (SYBR Green, Tiangen) under the following cycling conditions: 95°C for 30 seconds, 50°C for 30 seconds, and 72°C for 30 seconds for 40 cycles. The qRT-PCR primer sequences used are presented in the Table. The results are expressed as the mRNA fold change relative to that of the control group after normalization to the reference gene, *GAPDH*. Analyses were performed by calculating the relative expression using the $2^{-\Delta\Delta Ct}$ method.

Statistical Analyses

Data are presented as the mean ± SD. The differences between two groups were analyzed by unpaired *t*-test. Differences in three or more groups were analyzed by one-way ANOVA with Bonferroni correction. qRT-PCR data were

Investigative Ophthalmology & Visual Science

Table. Sequences of Primers for qRT-PCR

Gene	Primer Sequences
IL1B F	5′-CCTTGTGCAAGTGTCTGAAGC-3′
IL1B R	5′-CTCCACGGGCAAGACATAGG-3′
TNF F	5′-ACGTCGTAGCAAACCACCAA-3′
TNF R	5′-CAAGGGCTCTTGATGGCAGA-3′
MCP1 F	5′-CTGTCTCAGCCAGATGCAGTT-3′
MCP1 R	5′-GGTGCTGAAGTCCTTAGGGTT-3′
GAPDH F	5′-CTCTTGTGACAAAGTGGAC-3′
GAPDH R	5′-CCATTTGATGTTAGCGGGA-3′

analyzed with Prism 5 software (GraphPad, San Diego, CA, USA). Statistical significance was set at $P < 0.05$.

Results

Pyroptosis Was Activated in Retina After Experimental RD in Rats

To assess pyroptotic activation in detached retina, we subjected Brown-Norway rats to unilateral RD in the right eyes, and the left eyes served as controls. The retinas were collected at multiple time points after surgery followed by western blotting analysis. We found that the GSDMD-N moiety level increased abruptly after surgery, peaked at around 24 hours, and then gradually declined until day 7, the last tested time point (Figs. 1A, 1B). Consistently, the time course for caspase-1 activation followed a pattern similar to that for GSDMD activation (Figs. 1A, 1C). To further identify the localization of pyroptotic activation on retina 1 day after detachment, the rats were injected with TOTO-3 subretinally, and the retinas were collected for immunofluorescent detection. Notably, the TOTO-3-positive cells (Fig. 1D, red) were located at the ONL and colocalized with caspase-1 signal (Fig. 1D, green). Based on these results, we argue that pyroptosis is activated in the detached retina.

To assess retinal structures at the subcellular level, we applied TEM to image the detached retina. At 24 hours after RD, lytic structures (i.e., membranous ruptures, nuclear discontinuities, and cellular swelling) characteristic of pyroptotic or necrotic cell death were readily detected in the retinal ONL, whereas the apoptosis-specific structures were barely detected at this stage (Figs. 1E, 1G). However, 72 hours after RD, a marked increase in apoptotic signatures (i.e., cellular shrinkage and nuclear condensation) was noticed (Figs. 1F, 1G). These data are consistent with our hypothesis that pyroptosis is initiated early in the photoreceptors after RD followed by apoptotic activation.

GSDMD-C Preserved Photoreceptor Integrity After RD

The C-terminal moiety of GSDMD serves as a self-autonomous inhibitor of GSDMD activity.[13] It has been shown that GSDMD-C overexpression suppresses GSDMD-mediated pyroptosis in vitro.[13] To explore the functional outcome of GSDMD-C overexpression in the ONL after RD, we packaged recombinant AAV vectors to deliver a GSDMD-C expression cassette into the photoreceptors. Three weeks after viral treatment, the retinas were analyzed by histology. In general, GSDMD-C overexpression did not induce photoreceptor degeneration, as confirmed by H&E staining (Fig. 2A). We also noticed that GSDMD-C expression was detected predominantly in the ONL (Fig. 2B). In addition, we confirmed expression of exogenous GSDMD-C in the retina by western blotting (Fig. 2C). Virus-mediated eGFP expression was employed as control.

Next, we performed RD surgery in the virus-treated animals and asked whether GSDMD-C overexpression protects photoreceptors after RD. Although caspase-1 was activated in the detached retinas in all groups, GSDMD cleavage appeared to be perturbed by GSDMD-C overexpression as compared to vehicle and virus controls (Figs. 2D–2F). Because GSDMD-N serves as a building block of permeable membranous pores, we further employed TOTO-3 staining to evaluate the membrane integrity of retinal neurons after RD. We found that 24 hours after RD, when cellular membrane disruption was prominent, TOTO-3-positive photoreceptors were readily detected in the vehicle and virus control groups, and GSDMD-C overexpression significantly suppressed TOTO-3 penetration (Figs. 3A, 3B). Structural changes in photoreceptors were analyzed by TEM. Although lytic structures were readily detected in vehicle and virus controls, GSDMD-C overexpression significantly preserved the photoreceptor substructure 24 hours after RD (Figs. 3C, 3D). To further explore the potential effect on apoptotic death after pyroptosis inhibition, retinas were harvested 72 hours after RD and then subjected to TEM analysis. Interestingly, apoptotic features were drastically alleviated after GSDMD-C treatment (Figs. 3E, 3F). These data suggest that GSDMD-C overexpression preserves photoreceptor integrity and ameliorates subsequent apoptotic degeneration after RD.

Moreover, we assessed the effect of GSDMD-C overexpression in photoreceptors before and after experimental RD by ERG. The ERG assay was performed 7 days before and after RD surgery. Although the dark-adapted a-wave amplitudes were modestly retained in the control groups, approximately 65% recovery was recorded in the GSDMD-C treatment group (Figs. 4A, 4B). In addition, GSDMD-C overexpression in photoreceptors also rescued the b-wave amplitudes 7 days after RD (Figs. 4A, 4C). We further sectioned the retinal tissues for H&E analysis. The thickness of retina and ONL was measured to evaluate retinal structure. We found that the ONL was significantly preserved in the GSDMD-C treatment group as compared to controls (Figs. 4D–4F). Thus, we concluded that GSDMD-C overexpression rescued photoreceptors functionally after RD.

GSDMD-C Overexpression in Photoreceptors Attenuated Retinal Stress Response After RD

Retinal gliosis and inflammation have been documented as stress responses to RD. Here, we applied immunostaining against GFAP to assess Müller cell activation. As expected, longitudinal fiber-like signals were readily detected in the retina of the vehicle and virus controls 7 days after RD. In sharp contrast, GFAP activation was attenuated in the GSDMD-C treatment group (Figs. 5A, 5D). Moreover, we performed F4/80 and Iba-1 immunofluorescent staining to label macrophage and microglia on retinal sections. At 24 hours after RD, an amoeboid activated morphology was readily detected in the retinas in the vehicle and virus control groups, indicating inflammatory activation; however, GSDMD-C overexpression appeared to suppress macrophage and microglia activation (Figs. 5B–5F). Monocyte-derived inflammatory factors have been reported

Investigative Ophthalmology & Visual Science

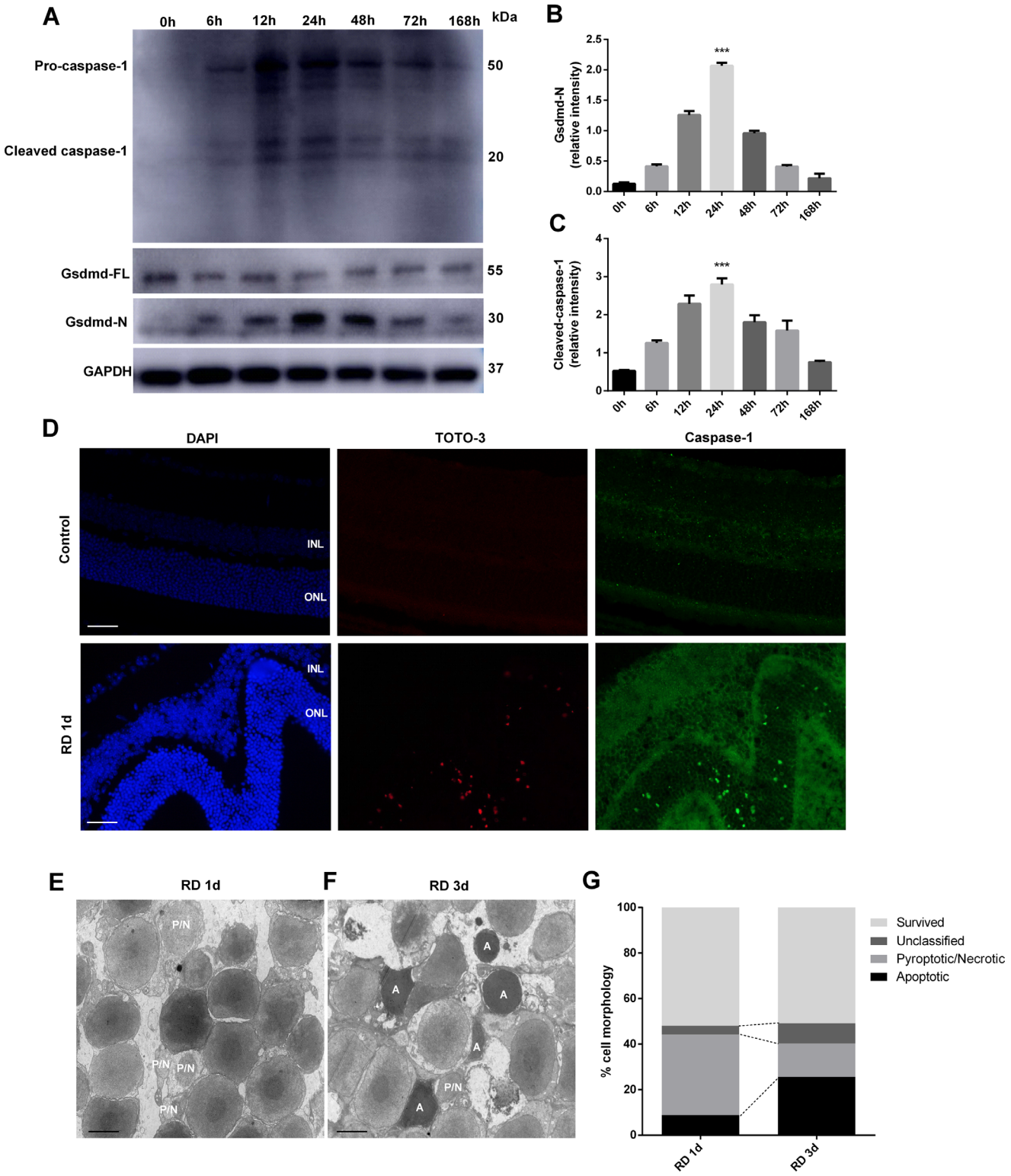

Figure 1. GSDMD and caspase-1 expression, TEM of photoreceptors 1 day and 3 days after RD, and TOTO-3 and caspase-1 staining 1 day after RD. (**A**) Time course of GSDMD-N, GSDMD-FL, and cleaved caspase-1 levels in rat retina, detected by western blotting at 0 hour (control eyes, $n = 6$) and from 6 to 168 hours after RD surgery ($n = 6$ per time point). (**B**, **C**) Densitometry analysis of the western blotting data normalized to the intensity of GAPDH ($n = 6$). Statistical analyses were performed via ANOVA with Bonferroni correction for the three independent experiments. Data are presented as the mean ± SD. (**D**) Representative TOTO-3 and caspase-1 staining of photoreceptors 1 day after RD ($n = 6$). *Scale bar*: 25 µm. (**E**, **F**) Representative TEM photographs of photoreceptors 1 day and 3 days after RD ($n = 6$). *Scale bar*: 2 µm. (**G**) Quantification of different cell death forms 1 day and 3 days after RD. $^{***}P < 0.001$. INL, inner nuclear layer; P/N, pyroptotic/necrotic; A, apoptotic.

Investigative Ophthalmology & Visual Science

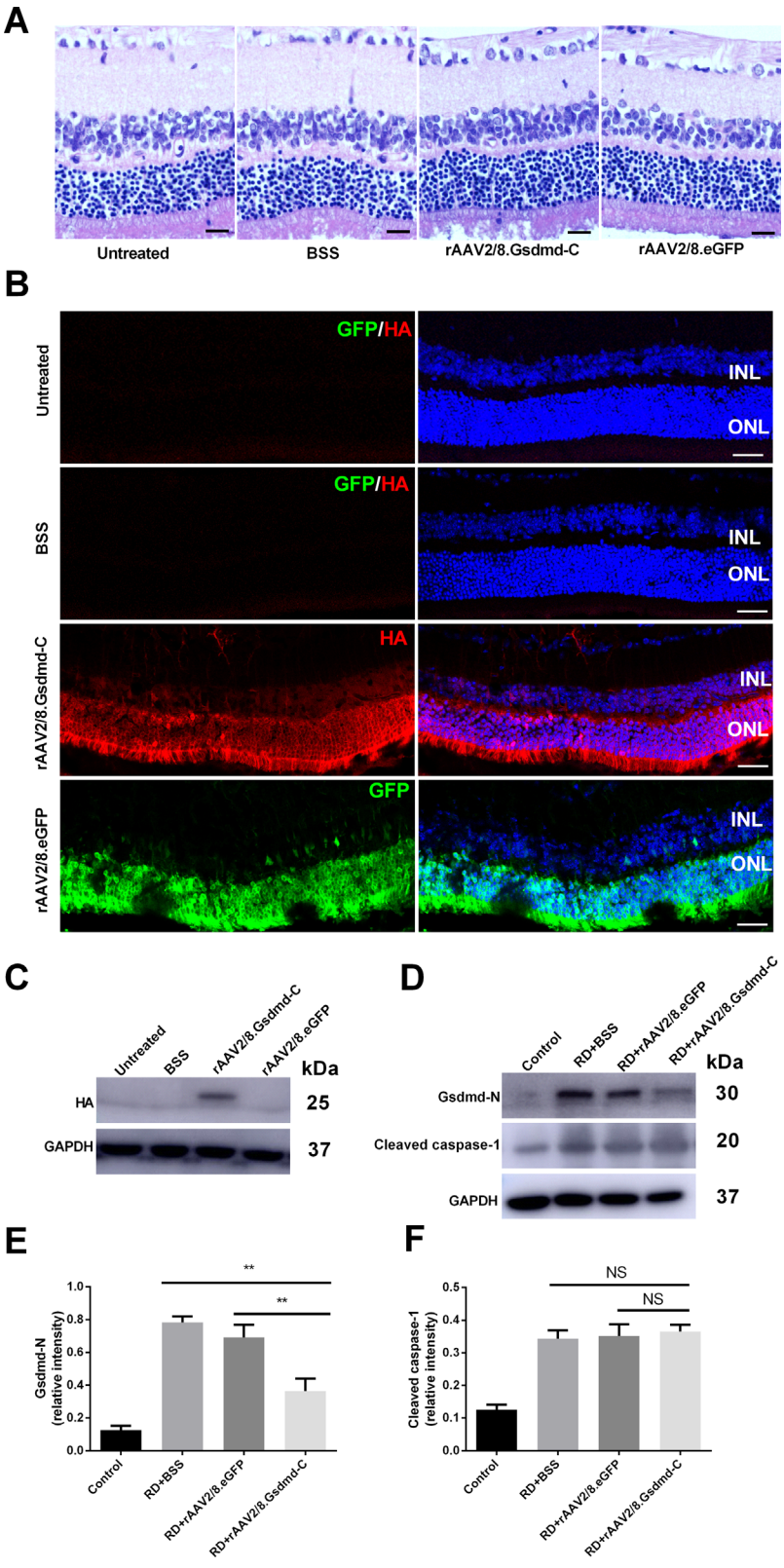

Figure 2. Morphological evaluation of subretinal injection and transfection efficiency of rAAV2/8–GSDMD-C. (**A**) Hematoxylin and eosin-stained retinal sections show retinal changes in the untreated, BSS, rAAV2/8–eGFP, and rAAV2/8–GSDMD-C groups 3 weeks after subretinal injection ($n = 6$). *Scale bars*: 25 µm. (**B**) Representative HA (*red*) and GFP (*green*) staining in rat retinal sections. Rat retinas were treated with BSS, rAAV2/8–GSDMD-C, or rAAV2/8–eGFP and assessed 3 weeks after subretinal injection ($n = 6$). *Scale bars*: 25 µm. (**C**) Western blotting analysis of the retinal lysates in all four groups ($n = 6$). (**D**) Western blotting analysis of the retinal lysates after RD in all four groups ($n = 6$). (**E**, **F**) Densitometry analysis of the western blotting data indicated that GSDMD-N decreased in the rAAV2/8–GSDMD-C-treated group 1 day after RD, and there was no significant difference for cleaved caspase-1 ($n = 6$). Data are expressed as the mean ± SD. Statistical analysis was performed via ANOVA with Bonferroni correction for the three independent experiments. $^{**}P < 0.01$. NS, not significant.

Investigative Ophthalmology & Visual Science

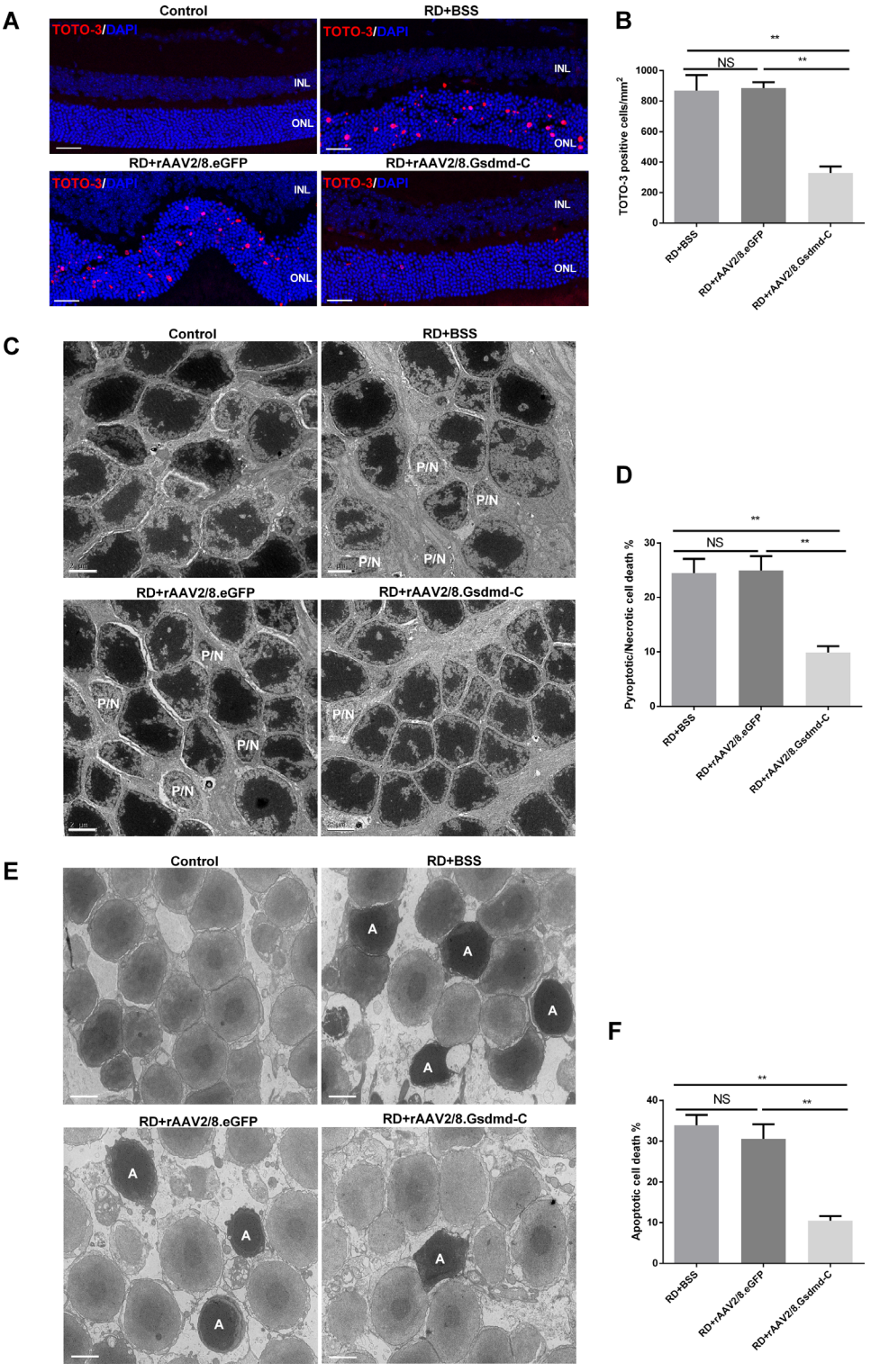

Figure 3. rAAV intervention of GSDMD-C prevents RD-induced photoreceptor pyroptosis and subsequent apoptosis. (**A**) Representative TOTO-3 iodide staining in the ONL 1 day after experimental RD in rats treated with BSS, rAAV2/8–GSDMD-C, or rAAV2/8–eGFP. DAPI staining was used to visualize the cell nuclei ($n = 6$). *Scale bars*: 25 µm. (**B**) Quantification of TOTO-3-positive cells 1 day after RD in all four groups ($n = 6$). Data are expressed as the mean ± SD. Statistical analysis was performed via ANOVA with Bonferroni correction for the three independent experiments. (**C**) Representative TEM photographs among the four groups 1 day after experimental RD ($n = 6$). *Scale bars*: 2 µm. (**D**) Quantification of pyroptotic/necrotic cell counts 1 day after RD in all four groups ($n = 6$). Data are expressed as the mean ± SD. Statistical analysis was performed via ANOVA with Bonferroni correction for the three independent experiments. (**E**) Representative TEM photographs among the four groups 3 days after experimental RD ($n = 6$). *Scale bars*: 2 µm. (**F**) Quantification of apoptotic cells counts 3 days after RD in all four groups ($n = 6$). Data are expressed as the mean ± SD. Statistical analysis was performed via ANOVA with Bonferroni correction for the three independent experiments. $^{**}P < 0.01$. NS, not significant; P/N, pyroptotic/necrotic; A, apoptotic.

Investigative Ophthalmology & Visual Science

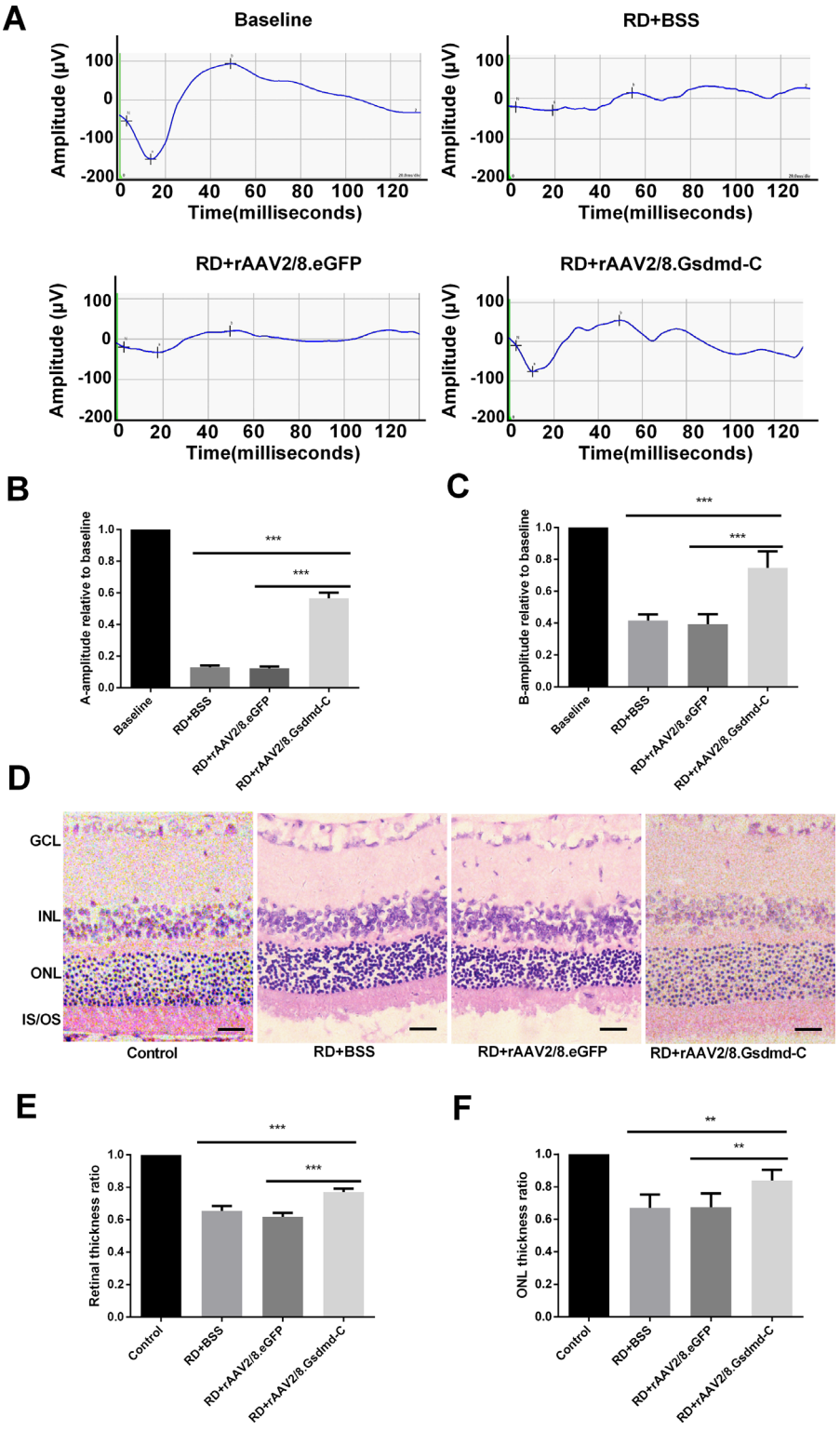

Figure 4. rAAV intervention of GSDMD-C preserves retinal functions and retinal morphology after RD. (**A**) ERGs were recorded in dark-adapted rats in the BSS, rAAV2/8–GSDMD-C, and rAAV2/8–eGFP groups 7 days after RD ($n = 6$). (**B**, **C**) Quantification of the amplitude of scotopic a- and b-waves; the amplitudes of a-waves and b-waves were reduced in all three groups, and rAAV2/8–GSDMD-C infection significantly rescued the retinal functions, as indicated by the increases in a-waves and b-waves ($n = 6$). Data are expressed as the mean ± SD. (**D**) Representative H&E-stained retinal sections present in the ONL of the retinas in all four groups 7 days after RD. Thickness of the ONL normalized to that of the INL was considered an indication of photoreceptor survival. *Scale bars*: 25 μm. (**E**, **F**) Quantification of retinal thickness and the ONL/INL thickness ratio. Compared with rats treated with BSS or rAAV2/8–eGFP, the rAAV2/8–GSDMD-C group showed a significant increase in retinal thickness and ONL/INL thickness ratio after RD ($n = 6$). Data are expressed as the mean ± SD. $^{**}P < 0.01$, $^{***}P < 0.001$.

Investigative Ophthalmology & Visual Science

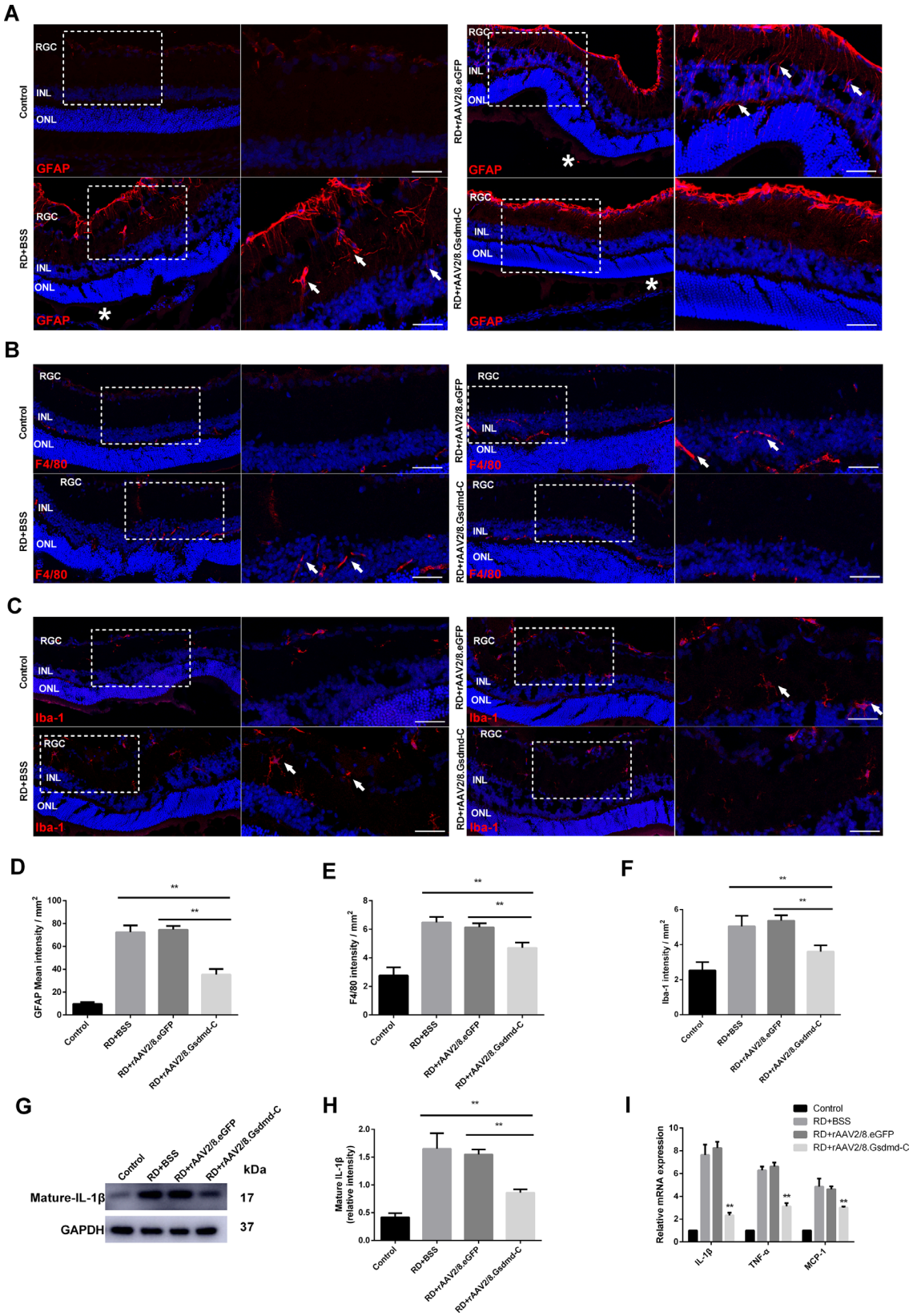

Figure 5. Involvement of rAAV2/8–GSDMD-C in the inflammatory response after RD. (**A**) Representative GFAP staining (*red*) in rat retinal sections. The eyes were treated with BSS, rAAV2/8–GSDMD-C, or rAAV2/8–eGFP and assessed 7 days after RD surgery ($n = 6$). DAPI was used to visualize the cell nuclei. *White arrows* indicate longitudinal fiber-like GFAP signals in the inner plexiform layer (IPL); *white asterisks* indicate separation points between detached and attached retina. *Scale bars*: 25 µm. (**B**) Representative F4/80 staining (*red*) in rat retinal sections. The eyes were treated with BSS, rAAV2/8–GSDMD-C, or rAAV2/8–eGFP and assessed 1 day after RD surgery ($n = 6$). DAPI was used

to visualize the cell nuclei. *White arrows* show the intensified F4/80 signal in the outer plexiform layer (OPL) and INL. (**C**) Representative Iba-1 staining (*red*) in rat retinal sections. The eyes were treated with vehicle BSS, rAAV2/8–GSDMD-C, or rAAV2/8–eGFP and assessed 1 day after RD surgery ($n = 6$). DAPI was used to visualize the cell nuclei. *White arrows* indicate the amoeboid-like Iba-1 signal in the IPL and retinal ganglion cells (RGCs). (**D–F**) Quantification of the immunofluorescence intensity in all four groups ($n = 6$). Data are expressed as the mean ± SD. Statistical analysis was performed via ANOVA with Bonferroni correction for the three independent experiments. (**G**) Western blotting analysis of mature IL-1β in retinal lysates 1 day after RD in all four groups ($n = 6$). (**H**) Densitometry analysis of the western blotting data indicated that mature IL-1β decreased in the rAAV2/8–GSDMD-C-treated group 1 day after RD ($n = 6$). Data are expressed as the mean ± SD. Statistical analysis was performed via ANOVA with Bonferroni correction for the three independent experiments. (**I**) mRNA levels of IL-1β, TNF-α, and MCP-1 were detected by qRT-PCR, and it was found that rAAV2/8–GSDMD-C treatment significantly reduced inflammatory factor transcription levels 1 day after RD ($n = 6$). $^{**}P < 0.01$.

to promote retinal degeneration.[19,20] Therefore, we further assessed IL-1β, MCP-1, and TNF-α expression in the retina by western blotting and qPCR. Although the expression of inflammatory cytokines was abruptly upregulated upon RD injury in the vehicle and virus control groups, attenuation of all tested cytokines was noticed only in the GSDMD-C treatment group (Figs. 5G–5I). Collectively, our data suggest that GSDMD-C overexpression in photoreceptors relieves the retinal stress upon RD injury.

Discussion

In this study, we showed that GSDMD, a critical mediator of pyroptosis, was constitutively expressed as a latent form in the retina and activated after experimental RD. Consistently, typical membranous rupture and bubbling structures that are characteristic of necroptosis or pyroptosis were noticed in the retinal ONL. In addition, overexpression of GSDMD-C in the photoreceptors preserved the ONL structurally and functionally and relieved retinal stress after experimental RD. Collectively, our findings suggest that pyroptosis is an alternative pathway through which photoreceptors degenerate after RD.

Multiple death pathways, including apoptosis, necrosis, and necroptosis, have been reported to mediate photoreceptor degeneration after RD.[8,21,22] Interestingly, inhibition of apoptosis induces receptor-interacting protein 1 (RIP1) phosphorylation and subsequent complex formation between RIP1 and RIP3, which is critical to necrosis activation.[23] These findings suggest that multiple death pathways could be orchestrated and switched under stressed conditions; however, understanding how photoreceptors regulate diverse degenerative pathways in response to injury remains elusive. Inflammation plays a significant role in retinal degeneration under disease conditions.[24,25] Tissue injury represents a functional damage-associated molecular pattern that activates inflammasome s NLRP3.[26] It has been shown that a NLRP3-dependent signaling cascade is activated in retina after experimental RD and plays a critical role in photoreceptor degeneration.[17] In recent years, it has been found that the NLRP3/caspase-1 axis is the upstream regulator of GSDMD-mediated pyroptosis; therefore, it would be of interest to determine whether photoreceptors degenerate through pyroptosis. Our data suggest that pyroptosis is a critical component of photoreceptor degeneration after RD.

How do photoreceptors initiate and regulate multiple pathways to execute cell death? TNF-α and Fas ligand (Fas-L) are potential regulators of both apoptotic and necrotic pathways.[27] The critical role of TNF-α in photoreceptor degeneration after RD has been validated.[28] Moreover, Fas-L/Fas is known to regulate photoreceptor death after RD[29,30] and may cooperate with TNF-α to activate RIP kinases and promote programmed necrosis in addition to apoptosis. RIPK3 was shown to regulate the necroptotic pathway and NLRP3 activation[31] and therefore served as a candidate. Moreover, recent studies have suggested that caspase-8 and mixed lineage kinase domain-like pseudokinase (MLKL), apoptotic effectors and executors of necroptosis, respectively, cross-talk with caspase-1- and GSDMD-mediated pyroptosis.[32,33] In our study, pyroptosis inhibition partly preserved subsequent apoptotic photoreceptor death in the RD model; however, the mechanism that manipulates pyroptosis-related apoptosis after RD remains unknown, although a complex interactive network may exist to regulate photoreceptor degeneration.

Tissue pyroptosis results in intracellular constituent release, including proinflammatory cytokines that potentially trigger local inflammation.[34] Retinal gliosis was shown to be activated by Müller cells. Activated monocytes are prominent locally in retinas releasing proinflammatory cytokines under disease conditions.[35,36] In our study, we found that inhibition of pyroptosis attenuated retinal gliosis and local cytokine expression, suggesting that photoreceptor pyroptosis after RD is a critical mechanism for initiating retinal stress responses. Furthermore, our findings highlight the therapeutic potential of targeting the pyroptotic pathway by GSDMD-C overexpression.

In summary, our study showed that the pyroptotic pathway was activated in the retina after experimental RD. We further demonstrated a protective effect of GSDMD-C overexpression in suppressing retinal inflammation and photoreceptor degeneration. Thus, GSDMD-mediated pyroptosis may serve as a therapeutic target for photoreceptor protection in retinal diseases.

Acknowledgments

The authors thank Genjie Ke, MD (Department of Ophthalmology, First Affiliated Hospital of USTC, University of Science and Technology of China) for his kind assistance with this study.

Supported by Grants from the National Science Fund for Distinguished Young Scholars (81425006, X. Sun); National Natural Science Foundation of China (81730026, X. Sun; 81700828, X. Luo); National Science and Technology Major Project for Drug Discovery of the Ministry of Science and Technology of China (2018ZX09301029-001, X. Sun); Biomedical Plan of Shanghai Science and Technology Committee (17411953000, X. Sun); Program for Eastern Young Scholar at Shanghai Institutions of Higher Learning (QD2016003, X. Luo); Science and Technology Commission of Shanghai Municipality (17140902800, W. Liu; 19YF1439800, T. Li); and National Key R&D Program of China (2016YFC0904800, X. Xu).

Disclosure: **X. Li,** None; **Y. Liu,** None; **M. Sun,** None; **M. Gao,** None; **T. Li,** None; **J. Liang,** None; **Y. Zhai,** None; **M. Xu,** None; **X. She,** None; **S. Yang,** None; **W. Liu,** None; **X. Luo,** None; **X. Sun,** None

References

1. Arroyo JG, Yang L, Bula D, Chen DF. Photoreceptor apoptosis in human retinal detachment. *Am J Ophthalmol*. 2005;139:605–610.
2. Mitry D, Awan MA, Borooah S, et al. Long-term visual acuity and the duration of macular detachment: findings from a prospective population-based study. *Br J Ophthalmol*. 2013;97:149–152.
3. Linsenmeier RA, Padnick-Silver L. Metabolic dependence of photoreceptors on the choroid in the normal and detached retina. *Invest Ophthalmol Vis Sci*. 2000;41:3117–3123.
4. Luo L, Uehara H, Zhang X, et al. Photoreceptor avascular privilege is shielded by soluble VEGF receptor-1. *Elife*. 2013;2:e00324.
5. Lo AC, Woo TT, Wong RL, Wong D. Apoptosis and other cell death mechanisms after retinal detachment: implications for photoreceptor rescue. *Ophthalmologica*. 2011;226(suppl 1):10–17.
6. Trichonas G, Murakami Y, Thanos A, et al. Receptor interacting protein kinases mediate retinal detachment-induced photoreceptor necrosis and compensate for inhibition of apoptosis. *Proc Natl Acad Sci U S A*. 2010;107:21695–21700.
7. Dong K, Han L, Liu J, Wang F, Sun X. RNA Interference reveals the coregulatory effects of cylindromatosis on apoptosis and necroptosis of photoreceptor cells in experimental retinal detachment. *Am J Pathol*. 2017;187:1763–1771.
8. Daruich A, Le Rouzic Q, Jonet L, et al. Iron is neurotoxic in retinal detachment and transferrin confers neuroprotection. *Sci Adv*. 2019;5:eaau9940.
9. Dong K, Zhu H, Song Z, et al. Necrostatin-1 protects photoreceptors from cell death and improves functional outcome after experimental retinal detachment. *Am J Pathol*. 2012;181:1634–1641.
10. Chen X, He WT, Hu L, et al. Pyroptosis is driven by non-selective gasdermin-D pore and its morphology is different from MLKL channel-mediated necroptosis. *Cell Res*. 2016;26:1007–1020.
11. Bergsbaken T, Fink SL, Cookson BT. Pyroptosis: host cell death and inflammation. *Nat Rev Microbiol*. 2009;7:99–109.
12. Shi J, Zhao Y, Wang Y, et al. Inflammatory caspases are innate immune receptors for intracellular LPS. *Nature*. 2014;514:187–192.
13. Shi J, Zhao Y, Wang K, et al. Cleavage of GSDMD by inflammatory caspases determines pyroptotic cell death. *Nature*. 2015;526:660–665.
14. Kayagaki N, Stowe IB, Lee BL, et al. Caspase-11 cleaves gasdermin D for non-canonical inflammasome signalling. *Nature*. 2015;526:666–671.
15. Evavold CL, Ruan J, Tan Y, Xia S, Wu H, Kagan JC. The pore-forming protein gasdermin D regulates interleukin-1 secretion from living macrophages. *Immunity*. 2018;48:35–44.e6.
16. Kuang S, Zheng J, Yang H, et al. Structure insight of GSDMD reveals the basis of GSDMD autoinhibition in cell pyroptosis. *Proc Natl Acad Sci USA*. 2017;114:10642–10647.
17. Kataoka K, Matsumoto H, Kaneko H, et al. Macrophage- and RIP3-dependent inflammasome activation exacerbates retinal detachment-induced photoreceptor cell death. *Cell Death Dis*. 2015;6:e1731.
18. She X, Lu X, Li T, et al. Inhibition of mitochondrial fission preserves photoreceptors after retinal detachment. *Am J Pathol*. 2018;188:1713–1722.
19. Wooff Y, Man SM, Aggio-Bruce R, Natoli R, Fernando N. IL-1 family members mediate cell death, inflammation and angiogenesis in retinal degenerative diseases. *Front Immunol*. 2019;10:1618.
20. Rutar M, Natoli R, Provis JM. Small interfering RNA-mediated suppression of Ccl2 in Müller cells attenuates microglial recruitment and photoreceptor death following retinal degeneration. *J Neuroinflammation*. 2012;9:221.
21. Murakami Y, Miller JW, Vavvas DG. RIP kinase-mediated necrosis as an alternative mechanisms of photoreceptor death. *Oncotarget*. 2011;2:497–509.
22. Huckfeldt RM, Vavvas DG. Neuroprotection for retinal detachment. *Int Ophthalmol Clin*. 2013;53:105–117.
23. Sun L, Wang H, Wang Z, et al. Mixed lineage kinase domain-like protein mediates necrosis signaling downstream of RIP3 kinase. *Cell*. 2012;148:213–227.
24. Murakami Y, Notomi S, Hisatomi T, et al. Photoreceptor cell death and rescue in retinal detachment and degenerations. *Prog Retin Eye Res*. 2013;37:114–140.
25. Sene A, Apte RS. Inflammation-induced photoreceptor cell death. *Adv Exp Med Biol*. 2018;1074:203–208.
26. Heneka MT, Kummer MP, Latz E. Innate immune activation in neurodegenerative disease. *Nat Rev Immunol*. 2014;14:463–477.
27. Degterev A, Huang Z, Boyce M, et al. Chemical inhibitor of nonapoptotic cell death with therapeutic potential for ischemic brain injury. *Nat Chem Biol*. 2005;1:112–119.
28. Xie J, Zhu R, Peng Y, et al. Tumor necrosis factor-alpha regulates photoreceptor cell autophagy after retinal detachment. *Sci Rep*. 2017;7:17108.
29. Zacks DN, Zheng QD, Han Y, Bakhru R, Miller JW. FAS-mediated apoptosis and its relation to intrinsic pathway activation in an experimental model of retinal detachment. *Invest Ophthalmol Vis Sci*. 2004;45:4563–4569.
30. Zacks DN, Boehlke C, Richards AL, Zheng QD. Role of the Fas-signaling pathway in photoreceptor neuroprotection. *Arch Ophthalmol*. 2007;125:1389–1395.
31. Vince JE, Wong WW, Gentle I, et al. Inhibitor of apoptosis proteins limit RIP3 kinase-dependent interleukin-1 activation. *Immunity*. 2012;36:215–227.
32. Orning P, Weng D, Starheim K, et al. Pathogen blockade of TAK1 triggers caspase-8-dependent cleavage of gasdermin D and cell death. *Science*. 2018;362:1064–1069.
33. Conos SA, Chen KW, De Nardo D, et al. Active MLKL triggers the NLRP3 inflammasome in a cell-intrinsic manner. *Proc Natl Acad Sci USA*. 2017;114:E961–E969.
34. Aglietti RA, Dueber EC. Recent insights into the molecular mechanisms underlying pyroptosis and gasdermin family functions. *Trends Immunol*. 2017;38:261–271.
35. Bringmann A, Pannicke T, Grosche J, et al. Müller cells in the healthy and diseased retina. *Prog Retin Eye Res*. 2006;25:397–424.
36. Kiang L, Ross BX, Yao J, et al. Vitreous cytokine expression and a murine model suggest a key role of microglia in the inflammatory response to retinal detachment. *Invest Ophthalmol Vis Sci*. 2018;59:3767–3778.

Investigative Ophthalmology & Visual Science